Chemical Vapor Deposition of Zirconium Oxide on Aerosolized Silicon Nanoparticles

Amanda M. Nienow and Jeffrey T. Roberts*

Department of Chemistry, University of Minnesota, 207 Pleasant Street Southeast, Minneapolis, Minnesota 55455

Received April 17, 2006. Revised Manuscript Received August 4, 2006

Nanoscale shells of ZrO_2 were deposited onto size-selected, aerosolized Si nanoparticles by chemical vapor deposition (CVD). The CVD precursor was nitronium pentanitratozirconate (ZN, $[NO_2][Zr(NO_3)_5]$), which has been used previously to deposit ZrO_2 films on silicon wafers. Silicon nanocrystals were synthesized from silane in a low-pressure nonthermal plasma and were directly extracted from the plasma growth chamber into an atmospheric-pressure aerosol flow tube reactor. The particle streams flowed first through a preheating furnace, which could be set between room temperature and 1000 °C, and then through a differential mobility diameter (DMA) that was set to transmit particles having a mobility diameter of 12 nm. After size selection, ZN was mixed into the carrier gas stream, and the resulting nanocrystal/ZN/carrier gas mixtures passed through a heated reaction zone ($T \approx 100$ °C), where deposition took place. The residence time in the reaction zone was approximately 8 s. The extent of deposition was determined by measuring the size distribution function of the postreaction aerosol with a second DMA. Particles were also analyzed by transmission electron microscopy (TEM). The measured changes in peak particle mobility diameter imply that at low-to-moderate ZN partial pressures (<100 Pa), the deposition rate is first-order in ZN partial pressure. At higher partial pressures, the rate increases more slowly with increasing ZN pressure. Possible reasons for these behaviors are discussed. The deposition rate increases with particle preheating temperature; the rate of particles that were preheated to 500 °C is roughly twice that of particles that are not preheated. This behavior is attributed to desorption of hydrogen from the particle surface leading to a more reactive substrate for CVD. We believe that these results are among the first in which CVD is used to coat size-selected, aerosolized nanoparticles and also among the first in which tandem differential mobility analysis (TDMA) is used to measure the rate of a CVD reaction.

I. Introduction

For nanoparticles to be useful in a wide variety of applications, methods must be developed to control their surface properties, for instance, by coating them with thin films to produce "core−shell" structures or by attaching functional groups to the surfaces. In some cases, the goal is to stabilize or passivate the particle surface; in other cases, it is to provide desired functionality. A variety of methods have been developed for coating and modifying nanoparticle surfaces. Whereas most work has involved liquid-solution-based chemistry, gas-phase (i.e., aerosol) methods are also being explored. Methods that are based on gas-phase particle manipulation offer several potential advantages, including (i) greater purity (solution-based methods often require the use of special solvent or catalyst that can deposit unwanted trace compounds or elements), (ii) the possibility of operating as continuous rather than batch processes, and (iii) the absence of environmentally hazardous solvents. Gas-phase methods are also obviously more compatible with systems in which the core nanoparticles are themselves synthesized in the gas phase. Gas-phase methods for particle coating that have been reported include heated flow tubes,[1] flames,[2] spray pyrolysis,[3] microwave plasma,[4] and RF plasma.[5]

We recently published a description of an apparatus that allows us to study the kinetics and mechanisms of reactions at the surfaces of aerosolized nanoparticles in an atmospheric-pressure aerosol flow tube reactor.[6−10] The apparatus is highly modular and can accept particles from virtually any aerosol source. The reaction zone is designed for maximal flexibility, with variable temperature (25−1200 °C), particle residence time (1−10 s), and gas-phase composition. One of the principle diagnostic tools is tandem differential mobility analysis (TDMA), in which monodisperse particle streams are created (selected diameters may be in the 5−40 nm range), subjected to chemical processing, and then analyzed

* To whom correspondence should be addressed. Telephone: (612) 624-1880. Fax: (612) 626-8659. E-mail: roberts@chem.umn.edu.

(1) Powell, Q. H.; Fotou, G. P.; Kodas, T. T.; Anderson, B. M. *Chem. Mater.* **1997**, *9*, 685−693.
(2) Zachariah, M. R.; Aquino, M. I.; Shull, R. D.; Steel, E. B. *Nanostruct. Mater.* **1995**, *5*, 383−92.
(3) Yu, F.; Wang, J. N.; Sheng, Z. M.; Su, L. F. *Carbon* **2005**, *43*, 3018−3021.
(4) Vollath, D.; Szabo, D. V. *J. Nanopart. Res.* **1999**, *1*, 235−242.
(5) Schallehn, M.; Winterer, M.; Weirich, T. E.; Keiderling, U.; Hahn, H. *Chem. Vap. Deposition* **2003**, *9*, 40−44.
(6) Liao, Y.-C.; Nienow, A. M.; Roberts, J. T. *J. Phys. Chem. B* **2006**, *110*, 6190−6197.
(7) Nienow, A. M.; Roberts, J. T.; Zachariah, M. R. *J. Phys. Chem. B* **2005**, *109*, 5561−5568.
(8) Higgins, K. J.; Jung, H.; Kittelson, D. B.; Roberts, J. T.; Zachariah, M. R. *Environ. Sci. Technol.* **2003**, *37*, 1949−1954.
(9) Higgins, K. J.; Jung, H.; Kittelson, D. B.; Roberts, J. T.; Zachariah, M. R. *J. Phys. Chem. A* **2002**, *106*, 96−103.
(10) Liao, Y.-C.; Roberts, J. T. *J. Am. Chem. Soc.* **2006**, *128*, 9061−9065.

10.1021/cm060883e CCC: $33.50
Published on Web 10/14/2006

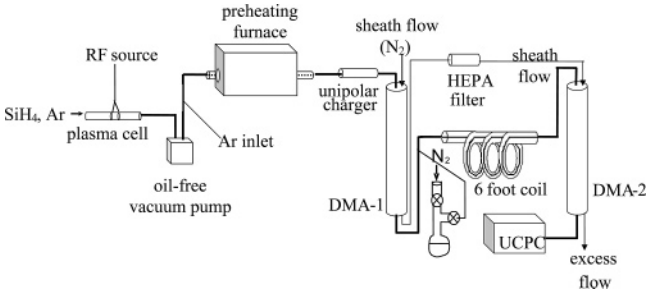

Figure 1. Schematic diagram of one configuration of the apparatus used for the experiments described in this work. The configuration shown was for experiments in which argon was the principle carrier gas and the particles were preheated. The bold line shows the path taken by the silicon particles.

for chemistry-induced changes in particle diameter (changes as small as 1% of the original diameter can be routinely measured). We have used this apparatus to study the surface oxidation kinetics of soot,[7−9] the thermal oxidation of silicon nanocrystals,[6] and the self-assembly of organic monolayers on silicon nanoparticles.[11] In the latter two studies, the silicon nanoparticles were extracted from a low-pressure plasma synthesis reactor.

In this paper, we describe a method for depositing zirconium dioxide (ZrO_2) layers onto size-selected, aerosolized silicon nanoparticles by chemical vapor deposition (CVD). The precursor to ZrO_2 was nitronium pentanitratozirconate (ZN, $[NO_2][Zr(NO_3)_5]$). There is considerable interest in incorporating silicon nanocrystals into devices for microelectronic, semiconductor, catalytic, and other applications,[12−14] but the majority of these applications will require the development of efficient strategies for surface coating, functionalization, or passivation. Zirconium dioxide was chosen as a coating material partly because of its desirable chemical and physical properties for some of the applications described above, e.g., chemical inertness and high index of refraction. Mostly, however, we deposited ZrO_2 because we have considerable experience with ZN as a precursor to ZrO_2 on Si wafers. We wanted to explore whether ZrO_2 coatings could be deposited onto aerosolized Si nanoparticles under conditions that are analogous to those used for deposition onto planar substrates.[15,16] Chemical vapor deposition has been used in the past to deposit shells onto aerosolized particles,[17] but not, to the best of our knowledge, on nanoparticles and not in a size-selected fashion.

II. Experimental Section

Deposition onto the silicon nanoparticles was carried out in an aerosol flow tube reactor. The apparatus, shown schematically in Figure 1, was a modified version of one described elsewhere.[6−9]

Table 1. Typical Experimental Conditions in TDMA-CVD System

condition	value
silane concentration	0.5% in He
silane flow rate	10 sccm
plasma pressure	25 ± 10 Torr
preheating temperature	RT−1000 °C
aerosol flow rate	1 L min^{-1}
sheath flow rate	10 L min^{-1}
D_p^0	12.2 nm
particle concentration at D_p^0	2.4×10^3/cc
geometric standard deviation	0.80
CVD reactor temperature	100 °C
N_2 flow rate in precursor vessel	0−100 sccm
precursor vessel temperature	85 °C
residence time in CVD reactor	∼8 s

In brief, the apparatus, which works at atmospheric pressure, is capable of accepting samples from virtually any aerosol source. The apparatus is equipped with two differential mobility analyzers (DMAs), one of which (DMA-1) is used to create monodisperse particle streams and the second of which (DMA-2) is used to reclassify an aerosol whose size characteristics have changed because of chemical or physical processing. The apparatus also has capabilities for electrostatic and inertial particle sampling onto transmission electron microscopy (TEM) grids. The operating conditions of the plasma, TDMA system, and CVD reactor are summarized in Table 1.

Silicon particles were synthesized from silane in a low-pressure (10−40 Torr), nonthermal plasma synthesis chamber.[6,11,18] Previous work has established that the particles are largely crystalline and the majority (>99%) are of nearly spherical shape (as verified by TEM analysis).[10] Particle size and morphology depend on the operating conditions of the plasma. For the experiments described in this paper, the most probable particle diameter (as measured by a differential mobility analyzer, DMA) was ∼12 nm. Particle samples were extracted as aerosols directly from the plasma chamber and immediately introduced into the flow tube reactor. Two methods were used to inject particles into the reactor, depending on the carrier gas. For nitrogen-based experiments, aerosol samples were extracted from the plasma and raised to atmospheric pressure using a nitrogen-operated vacuum pump (Air-Vac Engineering, model UV143H). For experiments in which argon was the carrier gas, aerosol samples were extracted using an oil-free vacuum pump (Welch, model 2561B-24), and argon was introduced downstream of the pump. Particles were introduced into the reactor at a carrier gas flow rate of ∼1 L min^{-1}.

Once in the flow tube, the particle streams passed through a preheating zone, which was a tube furnace (Lindberg, model HTF55122A, with a model 58114 temperature controller). The residence time in the furnace, which was only used for some of the experiments, was ∼0.5 s. The peak temperature could be adjusted between room temperature and 1000 °C. After leaving the preheating region, particles passed through a unipolar charger to establish a charge distribution on the aerosol,[19] and then through DMA-1 (TSI model 3085), which was set to transmit particles of a selected electric mobility diameter (typically, for these experiments, 12 nm). The unipolar charger was used to maximize the number of particles exiting the first DMA, and is of the same dimensions and operating conditions as that of Chen and Pui.[19]

The CVD precursor was mixed into the gas/particle stream immediately after mobility selection of the particles. ZN, which is a solid at room temperature, was synthesized from $ZrCl_4$ and N_2O_5 and purified by vacuum sublimation according to a published

(11) Liao, Y.-C.; Roberts, J. T. *Aerosol Sci. Technol.* **2006**, submitted.
(12) Dharmaprakash, M. S.; Shivashankar, S. A. *Mater. Res. Soc. Symp. Proc.* **2003**, *745*, 191−196.
(13) Forsgren, K.; Westlinder, J.; Lu, J.; Olsson, J.; Harsta, A. *Chem. Vap. Deposition* **2002**, *8*, 105−109.
(14) Cassir, M.; Goubin, F.; Bernay, C.; Vernoux, P.; Lincot, D. *Appl. Surf. Sci.* **2002**, *193*, 120−128.
(15) Burleson, D. J.; Gladfelter, W. L.; Campbell, S. A.; Roberts, J. T. *J. Electrochem. Soc.* **2002**, *149*, F131−F138.
(16) Smith, R. C.; Hoilien, N.; Taylor, C. J.; Ma, T.; Campbell, S. A.; Roberts, J. T.; Copel, M.; Buchanan, D. A.; Gribelyuk, M.; Gladfelter, W. L. *J. Electrochem. Soc.* **2000**, *147*, 3472−3476.
(17) Heel, A.; Kasper, G. *Aerosol Sci. Technol.* **2005**, *39*, 1027−1037.
(18) Mangolini, L.; Thimsen, E.; Kortshagen, U. *Nano Lett.* **2005**, *5*, 655−659.
(19) Chen, D.-R.; Pui, D. Y. H. *J. Nanopart. Res.* **1999**, *1*, 115−126.

procedure.[20] The air-sensitive compound was stored in a sealed vessel through which it was possible to flow high-purity (99.999%) nitrogen carrier gas. The carrier-gas flow rate was controlled using a mass flow controller (MKS, model 1259B) interfaced to a control box (MKS, model 247). So as to achieve an adequate ZN vapor pressure, we heated the precursor vessel with heating tape. The temperature of the vessel was measured by a thermometer.

Particle/ZN/carrier gas streams then passed into the reaction zone, which was a heated stainless steel coil, 2 m long and 0.6 cm in diameter. Under the flow conditions used for this work, the residence time in the heated zone was approximately 8 s. The coil was wrapped with a Variac-controlled heating tape, which allowed for control of the reaction temperature.

ZN thermally decomposed on the Si particles in the reaction zone to deposit a thin oxide coating. The increase in particle diameter that resulted from the formation of this coating was measured using a second DMA. The postreaction particle stream was reclassified using DMA-2 (TSI, model 3085). Particles were detected with an ultra-fine condensation particle counter (UCPC, TSI model 3025A). The high-voltage supply for DMA-2 was programmed remotely using a PC with a multifunction board (National Instruments Lab-PC+) with a 12 bit D/A converter under software control. Scans were performed by incrementing the particle size by 0.2 nm, waiting 8 s for the flow to stabilize, and then collecting 3 readings from the UCPC at 2 s intervals. Chen and Kesten measured the size-dependent transmission efficiency of the nano-DMA model used for DMA-2, as well as the size-dependent counting efficiency of the UCPC.[21,22] These measurements were used to correct the size distribution measurements. For the T-DMA scans, peaks in the corrected particle size distributions were fit to normal Gaussian functions using the Levenberg−Marquardt algorithm.[23] The center of the Gaussian function was taken as the most probable particle size.

Particles were collected for transmission electron microscopy (TEM) and energy-dispersive X-ray (EDX) analysis using Tecnai T12 and G30 microscopes. Samples were collected immediately after mobility classification by DMA-1 and after passing through the reaction zone. Particles were collected by electrostatic sampling onto 3 mm lacey carbon-coated copper TEM grids. The grids were taped to a grounded stainless steel cylinder inserted into a Teflon Swagelok tee. A copper wire was applied to the top of the Swagelok tee, and a potential between +1 and +3 kV was applied to the wire. Sampling times were typically between 30 and 120 min. Samples were transported to the microscopes as quickly as possible so as to reduce the possibility of coating degradation.

III. Results

The extent of CVD was monitored by tandem differential mobility analysis (TDMA). In TDMA, an initially monodisperse particle stream is subjected to chemical or physical processing, and the size changes that result from this processing are determined by remeasuring the particle size distribution.[24−27] Figure 2 shows a representative set of data.

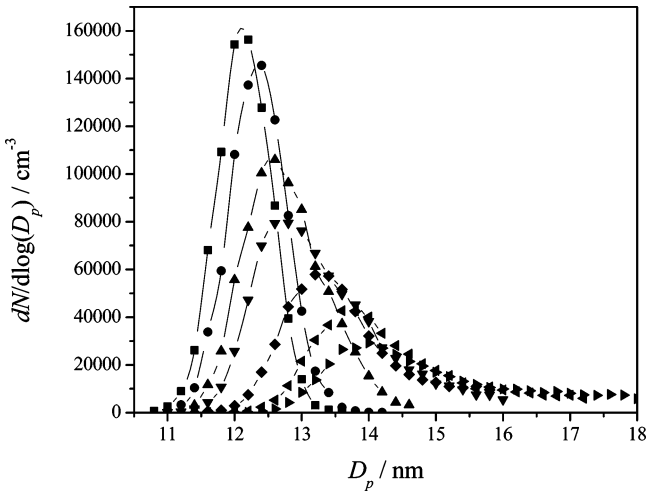

Figure 2. Representative set of TDMA scans of 12 nm initial mobility diameter silicon particles after interaction with ZN. The lines are the best-fit Gaussian distributions. The symbols refer to the different N_2 flow rates through the ZN vessel: 0 (■), 5 (●), 10 (▲), 15 (▼), 40 (◆), 70 (left-facing solid triangle), and 100 (right-facing solid triangle) sccm N_2. The temperature of the precursor vessel was 85 °C, and the temperature in the reaction coil was 100 °C.

In this set of experiments, the initially selected particle mobility diameter, $\bar{D}_p^i$, was 12 nm, and N_2 was used as the carrier gas through the entire flow tube. The ZN vessel was heated to 85 °C, and the stainless steel reaction coil was maintained at 100 °C. The series of scans shows how particle growth depends on Q_{ZN}, the volumetric N_2 flow rate through the ZN vessel. For these experiments, Q_{ZN} was varied between 0 (i.e., when there was no ZN introduction into the flow tube) and 100 sccm.

As expected, under conditions of no ZN introduction into the heated aerosol flow tube ($T = 100$ °C), the peak diameter is unchanged from the initially selected value of 12 nm. However, when ZN is introduced, the peak mobility diameter ($\bar{D}_p$) increases, with the extent of increase depending on Q_{ZN}. Under the highest flow rate conditions investigated ($Q_{ZN} =$ 100 sccm N_2), the most probable diameter increases by 1.8 nm, which suggests a coating ~0.9 nm thick. The particle distributions of coated particle streams are broader than those of the uncoated particles and the peak heights are reduced. The integrated peak areas are constant, however, which indicates that particle numbers are conserved in these experiments. At high N_2 flow rates (>20 sccm), the particles size distributions become skewed, and there are long tails in the distributions in the direction of high mobility diameters. This skewing of the distribution is discussed below.

A series of blank experiments was conducted in which the plasma reactor was turned off, so that no silicon particles were introduced into the flow tube, but ZN was introduced into the flow tube (~100 °C) as described above. Under these conditions, no particles <75 nm in mobility diameter were observed. This demonstrates that ZN does not self-nucleate to form particles in the 3−75 nm range. The tails in the TDMA traces are therefore not due to the formation of Zr or ZrO_2 particles from ZN decomposition. As will be

(20) Field, B. O.; Hardy, C. J. *Proc. Chem. Soc.* **1962**, 76−7.
(21) Chen, D. R.; Pui, D. Y. H.; Hummes, D.; Fissan, H.; Quant, F. R.; Sem, G. J. *J. Aerosol Sci.* **1998**, *29*, 497−509.
(22) Kesten, J.; Reineking, A.; Porstendorfer, J. *Aerosol Sci. Technol.* **1991**, *15*, 107−111.
(23) Bates, D. M.; Watts, D. G. *Nonlinear Regression and Its Applications*; Wiley: New York, 1988.
(24) Knutson, E. O.; Whitby, K. T. *J. Aerosol Sci.* **1976**, *6*, 443−51.
(25) Liu, B. Y. H.; Pui, D. Y. H.; Whitby, K. T.; Kittelson, D. B.; Kousaka, Y.; McKenzie, R. L. *Atmos. Environ. (1967−1989)* **1978**, *12*, 99−104.
(26) Rader, D. J.; McMurry, P. H. *J. Aerosol Sci.* **1986**, *17*, 771−87.
(27) McMurry, P. H.; Stolzenburg, M. R. *Atmos. Environ. (1967−1989)* **1989**, *23*, 497−507.

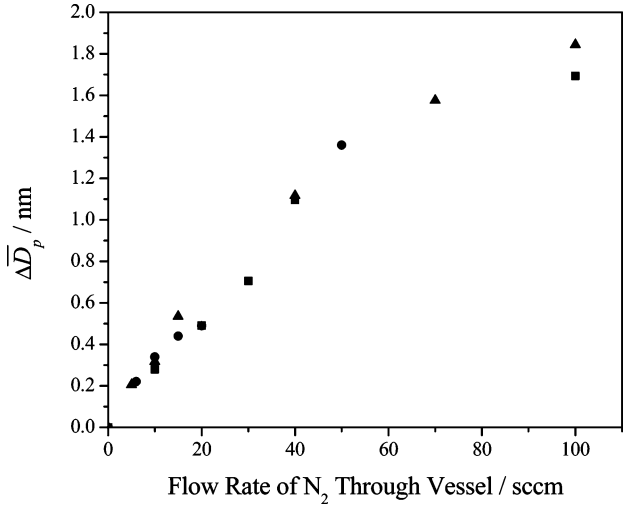

Figure 3. Measured changes in peak particle mobility diameter ($\Delta\bar{D}_p$) after interaction with ZN, as a function of nitrogen flow rate through the ZN vessel. The temperature of the precursor vessel was 85 °C, and the temperature in the reaction coil was 100 °C. Results from three sets of experiments conducted on three different days are displayed, as indicated by ▲, ●, and ■.

discussed below, some much larger (>200 nm diameter) Zr-containing particles were observed by TEM/EDX, but these sizes are out of the range of our TDMA scans. The mechanism of formation of these large particles in unclear, but it is not likely due to agglomeration of coated particles as all of the particles are negatively charged.

Several sets of TDMA scans were obtained over a broad range of N_2 flow rates over a one-month period. Figure 3, which plots the change in peak mobility diameter ($-\bar{D}_p = \bar{D}_p - \bar{D}_p^i$) against the N_2 flow rate through the ZN vessel, summarizes the results of these experiments. From Figure 3, it is apparent that $\Delta\bar{D}_p$ varies linearly with N_2 flow rate up to ~60 sccm. Beyond 60 sccm, $\Delta\bar{D}_p$ continues to increase monotonically with flow rate, but in a nonlinear fashion and at a slower rate than below 60 sccm. The plotted results are from three different sets of experiments, with each set recorded on a different day. The high level of agreement between the different data sets indicates a measure of the reproducibility of these experiments.

The silicon nanoparticles are produced in a hydrogen-rich environment. Infrared spectra of collected particles clearly indicate the presence of Si−H bonds at the particle surface, although the surface hydrogen coverage has not been determined.[11] In previous work on ZrO_2 CVD from ZN on silicon wafers, the wafers were heated prior to deposition so as to desorb surface hydrogen.[28,29] To assess the potential role of adsorbed hydrogen in the nanoparticle system, we conducted experiments in which the silicon particle streams were preheated before the initial mobility classification step. In Figure 4, we show how $\Delta\bar{D}_p$ varies with the preheating oven setting (which is equal, within 10 °C, to the maximum temperature in the preheating region). These data were obtained under conditions of 100 °C in the reaction zone,

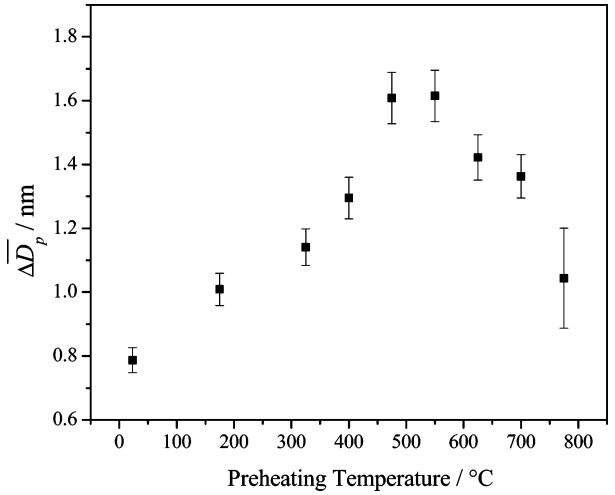

Figure 4. Measured changes in peak particle mobility diameter ($\Delta\bar{D}_p$) after interaction with ZN, as a function of the preheating temperature in N_2 carrier gas. The temperature of the precursor vessel was 85 °C, the temperature in the reaction coil was 100 °C, and the carrier-gas flow rate through the ZN vessel was 50 sccm. Error bars are shown.

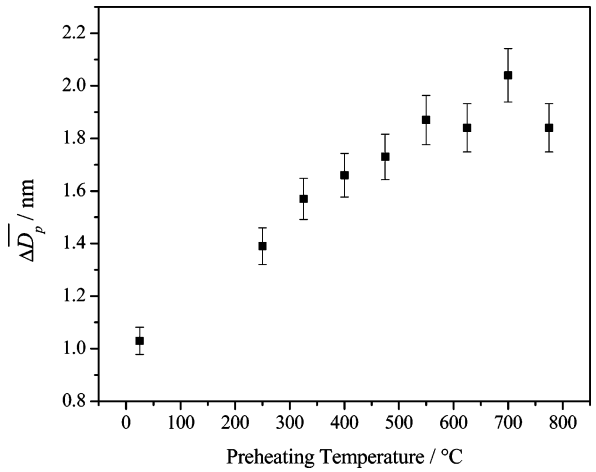

Figure 5. Measured changes in peak particle mobility diameter ($\Delta\bar{D}_p$) after interaction with ZN, as a function of the preheating temperature in N_2 carrier gas. The temperature of the precursor vessel was 85 °C, the temperature in the reaction coil was 100 °C, and the carrier-gas flow rate through the ZN vessel was 50 sccm. Error bars are shown.

85 °C in the precursor vessel, and N_2 flow throughout the reactor. The nitrogen flow rate through the ZN vessel was 50 sccm. Clearly, the extent of growth depends on the preheating temperature, with $\Delta\bar{D}_p$ increasing monotonically with preheating temperature up to ~500 °C (from 0.8 nm at room temperature to 1.6 nm at 500 °C), at which point the temperature $\Delta\bar{D}_p$ begins to decrease with increasing preheating temperature. Possible reasons for this behavior will be discussed below.

To determine whether N_2 reacts with an aerosolized Si nanoparticle, we studied the influence of carrier gas in the preheating region. A set of experiments analogous to those described immediately above was conducted, except that Ar rather than N_2 was used as the carrier gas through the flow tube. (Nitrogen continued to be used as the carrier gas through the ZN vessel, but its introduction occurred after the preheating and initial mobility classification steps.) Figure 5 shows the results of those experiments. As is the case when particles are preheated in N_2, $\Delta\bar{D}_p$ increases with preheating temperature up to 500 °C. The amount of growth is equal,

(28) Burleson, D. J.; Roberts, J. T.; Gladfelter, W. L.; Cambell, S. A.; Smith, R. C. *Proc. Electrochem. Soc.* **2001**, *2001−13*, 144−151.
(29) Smith, R. C.; Ma, T.; Hoilien, N.; Tsung, L. Y.; Bevan, M. J.; Colombo, L.; Roberts, J.; Campbell, S. A.; Gladfelter, W. L. *Adv. Mater. Opt. Electron.* **2000**, *10*, 105−114.

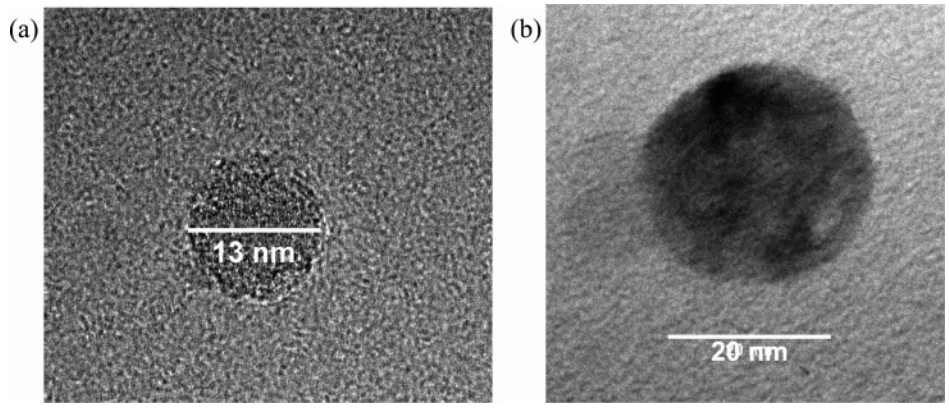

Figure 6. TEM images of silicon nanoparticles size-selected with a differential mobility analyzer. (a) Uncoated silicon nanoparticle selected with DMA set for 13 nm particles. Image taken with Tecnai G2 30 TEM; (b) 13 nm silicon nanoparticle after exposure to nitronium pentanitratozirconate. The particle diameter is slightly larger than 20 nm. Image taken with Tecnai T12 TEM on the same day as sample preparation.

within the experimental uncertainty, to what is observed in N_2. Above 500 °C, however, differences emerge. Specifically, $\Delta\bar{D}_p$ is roughly independent of the preheating temperature above 500 °C in Ar, whereas in N_2, $\Delta\bar{D}_p$ decreases with increasing preheating temperature above 500 °C. Possible reasons for this behavior will be discussed below.

Figure 6 shows representative TEM images of (a) uncoated and (b) coated 12 nm initial mobility diameter particles. Particles were coated in N_2 carrier gas; the N_2 flow rate through the ZN vessel was 100 sccm, the ZN vessel temperature was 85 °C, and the temperature in the reaction zone was 100 °C. As can be seen from the figure, the particles are spherical (as were all observed particles) and the coated particles are clearly larger (~22 nm in diameter) than the uncoated particles (~13 nm in diameter). In addition, no needlelike or other nonuniform ZrO_2 coating was observed. The particles shown in these images are larger than what one would expect on the basis of the peak maxima in the TDMA scans. We believe this is due mostly to sample bias: the electrostatic sampler preferentially collects larger particles over smaller ones. The collection efficiency of the sampler was very low, and we have relatively few images of particles (hence the somewhat poor quality of the images in Figure 6). However, these other images show particles with sizes closer to those predicted from the TDMA scans. Unfortunately, because of the small particle size and low particle concentrations on the TEM grids, no elemental analysis has been obtained at this point and no statistics could be collected to validate the polydispersity obtained from the T-DMA. The composition of the coating is therefore unknown, but on the basis of the known CVD chemistry in Si wafer systems, we presume the coating to be some form of ZrO_2.

IV. Discussion

A. Growth Kinetics. The N_2 flow rate through the ZN vessel controls the partial pressure of ZN in the reaction zone. If it is assumed that N_2 becomes saturated with ZN as it flows through the vessel, then P_{ZN}, the maximum partial pressure of ZN in the reaction coil, can be estimated

$$P_{ZN} = P^0_{ZN}\frac{Q_{ZN}}{Q_{total}} \tag{1}$$

where P^0_{ZN} is the equilibrium ZN vapor pressure and Q_{total} is the total volumetric flow rate in the reaction coil. The ZN vapor pressure has been measured to be between 50 and 110 °C and fit to a Clausius−Clapeyron expression.[30] We estimate that P^0_{ZN} at 85 °C (the temperature of the ZN vessel) is 1.6×10^3 Pa. The total volumetric flow rate is just the sum of Q_{ZN} and the total volumetric flow rate immediately prior to ZN mixing, which was 1000 sccm. We therefore estimate that P_{ZN} depends linearly on Q_{ZN}, from 0 Pa at $Q_{ZN} = 0$ sccm to 150 Pa at $Q_{ZN} = 100$ sccm. The actual ZN partial pressures may be lower than these estimated values because of a lack of N_2 saturation by ZN (especially at high values of Q_{ZN}) and reactive or absorptive loss of ZN during transport into the reaction coil.

The simplest plausible kinetic scheme for this system is one involving surface-limited growth and a single, first-order decomposition step, analogous to the system used to describe the formation of ZrO_2 layers on Si wafers. In this kinetic scheme, ZN molecules absorb intact (the molecule is stable in the gas-phase under the experimental conditions), sticks to the surface, and decomposes. Under such conditions, the CVD rate, expressed as dn_{ZrO_2}/dt (the change in number of moles of deposited ZrO_2 with respect to time) can be written as

$$\frac{dn_{ZrO_2}}{dt} = k_{CVD}Z_{ZN}\sigma \tag{2}$$

where k_{CVD} is the rate constant for ZN decomposition onto the CVD growth surface, Z_{ZN} is the collision rate between ZN (in units of mol cm^{-2} s^{-1}), and σ is the particle surface area.[6] For a spherical particle of diameter D_p, the rate of ZrO_2 accumulation can be related to the rate of diameter increase through the molar density of deposited material ($\bar{\rho}_{ZrO_2}$), and eq 2 may be rewritten as[6]

$$\frac{dD_p}{dt} = \frac{2\rho k_{CVD}\rho Z_{ZN}}{\bar{\rho}_{ZrO_2}} \tag{3}$$

The gas−surface collision rate is proportional to pressure under constant temperature conditions. Equation 3 therefore predicts that $\Delta\bar{D}_p$ varies linearly with Q_{ZN}. For low-to-

(30) Rees, W. 2006, personal communication.

moderate flow rates (up to $Q_{ZN} = 60$ sccm), Figure 3 shows that this situation prevails for ZN CVD onto aerosolized silicon nanoparticles that are not preheated. Beyond 60 sccm, however, the growth rate begins to increase much less rapidly, if at all, as additional ZN is added into the gas stream. The reason for this behavior is unclear. One possibility is that the kinetic scheme described above is overly simplistic, and that deposition involves two or more elementary reaction steps. Another is that N_2 does not become saturated with ZN under high flow rate conditions, so that Q_{ZN} is no longer proportional to P_{ZN}. Additional work is underway, including measurements of the deposition rate as a function of the coil reaction temperature and a more thorough characterization of the gas composition, which will help resolve the origin of nonlinear deposition rates under a high N_2 flow rate.

Because the growth rate was not measured as a function of temperature, we cannot determine the values of the Arrhenius parameters associated with k_{CVD}. We can, however, estimate the fraction of ZN molecules that decompose on a particle surface. If every ZN molecule that collides with a particle reacts to form ZrO_2, k_{CVD}, as defined in eq 2, is equal to 1. Therefore, for a particle spending time Δt in the reaction coil, the maximum change in particle diameter, $\Delta\bar{D}_p^{max}$, is given by

$$\Delta D_p^{max} = \frac{2Z_{ZN}}{\bar{\rho}_{ZrO_2}}\Delta t \qquad (4)$$

Under the flow conditions investigated in this work, Δt was $\sim$8 s. The various allotropes of ZrO_2 have different densities; we will assume a density of 0.05 mol cm^{-3}, which is midway between the densities of the monoclinic and tetragonal phases. The gas−surface collision rate can be calculated from gas kinetic theory. Using eq 4 and the measurements reported above, we estimate that $\Delta\bar{D}_p/\Delta\bar{D}_p^{max}$ in the low-to-moderate flow rate regime is $\sim 3 \times 10^{-6}$ for particles that are not preheated. Thus, roughly 1 in 300 000 ZN−surface collisions leads to the formation of CVD product.

B. Particle Preheating. The particle preheating experiments (in which particles were heated in N_2 or Ar prior to the introduction of precursor) establish that preheating leads to enhanced deposition from the ZN precursor. The rate enhancement (as manifested in higher $\Delta\bar{D}_p$ values) depends on the preheating temperature and is especially pronounced for preheating temperatures >350 °C. For preheating temperatures less than $\sim$500 °C, the enhancement obtained by preheating in N_2 is essentially the same as that obtained by preheating in Ar, with a monotonically increasing $\Delta\bar{D}_p$ value, from $\sim 0.9 \pm 0.1$ nm for no preheating to $\sim 1.7 \pm 0.1$ nm for preheating at 500 °C. Heating above 500 °C in Ar leads to no additional enhancement, and $\Delta\bar{D}_p$ remains constant at $\sim 1.7 \pm 0.1$ nm. Preheating above 500 °C in N_2, however, causes the deposition rate to decrease from $\sim 1.7 \pm 0.1$ nm at 500 °C to 1.0 ± 0.1 nm at 750 °C.

We believe that the preheating effect has its origins in hydrogen desorption. The silicon particles studied in this work are grown in a hydrogen-rich environment, and it is reasonable to assume that the particles leave the plasma reactor with adsorbed hydrogen. Indeed, the presence of adsorbed hydrogen has been demonstrated by infrared spectroscopy, although the coverage has not been quantified.[11] Although reports have appeared on the state of adsorbed hydrogen on Si nanocrystals,[31] there is, to the best of our knowledge, no published work on the thermal desorption of hydrogen from such a surface. There is a rich literature on the thermal desorption of hydrogen from single-crystal Si and from Si wafers. In general, hydrogen thermally desorbs from Si in the 450−700 °C range, with the desorption temperature depending on the state of the surface and the experimental conditions.[32−39] This brackets the range for which the preheating induced effect is most pronounced.

The presence or absence of a hydrogen capping layer is known to have a profound influence on the chemical properties of a silicon surface.[40−53] In some cases, adsorbed hydrogen acts as a passivation layer by terminating dangling bonds at the surface.[52] In others, adsorbed hydrogen increases surface reactivity because surface Si−H bonds can react in ways that a bare Si surface cannot.[54] We suggest that in the present system, adsorbed hydrogen is a passivation agent. Adsorbed hydrogen leads to decreased deposition because it slows nucleation during the initial phase of ZrO_2 deposition. The nucleation sites may be dangling bonds, or they may be sites at a reconstructed surface that forms after hydrogen desorption.

At high preheating temperatures (<500 °C), the particle growth rate decreases upon preheating in N_2 but not in Ar.

(31) Zhou, Z.; Brus, L.; Friesner, R. *Nano Lett.* **2003**, *3*, 163−167.
(32) Burton, L. C. *J. Appl. Phys.* **1972**, *43*, 232−3.
(33) Jin, X.; Feng, Y.; Zhuang, C.; Wang, X. *Wuli Xuebao* **1984**, *33*, 747−54.
(34) Gupta, A.; Tang, D.; McMurry, P. H. *J. Atmos. Chem.* **1995**, *20*, 117−39.
(35) Zou, J.; Baldwin, R. K.; Pettigrew, K. A.; Kauzlarich, S. M. *Nano Lett.* **2004**, *4*, 1181−1186.
(36) Greenlief, C. M.; Liehr, M. *Appl. Phys. Lett.* **1994**, *64*, 601−603.
(37) Sridhar, N.; Chung, D. D. L.; Anderson, W. A.; Yu, W. Y.; Fu, L. P.; Petrou, A.; Coleman, J. *Mater. Res. Soc. Symp. Proc.* **1994**, *321*, 713−18.
(38) Morita, Y.; Miki, K.; Tokumoto, H. *Surf. Sci.* **1995**, *325*, 21−32.
(39) Doren, D. J. *Adv. Chem. Phys.* **1996**, *95*, 1−60.
(40) Stockhausen, A.; Kampen, T. U.; Moench, W. *Appl. Surf. Sci.* **1992**, *56−58*, 795−801.
(41) Linford, M. R.; Chidsey, C. E. D. *J. Am. Chem. Soc.* **1993**, *115*, 12631−12632.
(42) Linford, M. R. Ph.D. Thesis, Stanford University, Stanford, CA, 1996.
(43) Kosugi, T.; Ishii, H.; Arita, Y. *J. Vac. Sci. Technol., A* **1997**, *15*, 127−132.
(44) Boukherroub, R.; Morin, S.; Sharpe, P.; Wayner, D. D. M.; Allongue, P. *Langmuir* **2000**, *16*, 7429−7434.
(45) Cicero, R. L.; Linford, M. R.; Chidsey, C. E. D. *Langmuir* **2000**, *16*, 5688−5695.
(46) Cicero, R. L.; Chidsey, C. E. D.; Lopinski, G. P.; Wayner, D. D. M.; Wolkow, R. A. *Langmuir* **2002**, *18*, 305−307.
(47) Quayum, M. E.; Kondo, T.; Nihonyanagi, S.; Miyamoto, D.; Uosaki, K. *Chem. Lett.* **2002**, 208−209.
(48) Wayner, D. D. M.; Wolkow, R. A. *J. Chem. Soc., Perkin Trans. 1* **2002**, 23−34.
(49) Boecking, T.; James, M.; Coster, H. G. L.; Chilcott, T. C.; Barrow, K. D. *Langmuir* **2004**, *20*, 9227−9235.
(50) Miramond, C.; Vuillaume, D. *J. Appl. Phys.* **2004**, *96*, 1529−1536.
(51) Sun, Q.-Y.; de Smet, L. C. P. M.; van Lagen, B.; Wright, A.; Zuilhof, H.; Sudhoelter, E. J. R. *Angew. Chem., Int. Ed.* **2004**, *43*, 1352−1355.
(52) Ma, L.; Wang, J.; Lu, Q.; Wang, G. *Chem. Phys. Lett.* **2005**, *405*, 208−213.
(53) Sun, Q.-Y.; De Smet, L. C. P. M.; Van Lagen, B.; Giesbers, M.; Thuene, P. C.; Van Engelenburg, J.; De Wolf, F. A.; Zuilhof, H.; Sudhoelter, E. J. R. *J. Am. Chem. Soc.* **2005**, *127*, 2514−2523.
(54) Hua, F.; Swihart, M. T.; Ruckenstein, E. *Langmuir* **2005**, *21*, 6054−6062.

One explanation for this observation is that N_2 reacts with the surface of an aerosolized Si particle to form a silicon nitride passivation layer. It has been shown that thin layers (~0.5 nm) of silicon nitride are formed on Si(001) and Si(111) when they are exposed to N_2 or N_2/H_2 mixtures at temperatures between 600 and 1100 °C.[55,56] Another possibility is that the particles are oxidized by O_2 that enters the reaction zone either through a leak or as an impurity in the liquid nitrogen tank (the stated O_2 level is 8 ppm). It should be noted in support of this hypothesis that the Ar tank had a lower stated O_2 concentration, and that a different method was used to extract particles into the TDMA system when Ar was the carrier gas. Work is ongoing to determine the origin of the CVD rate reduction that accompanies preheating in N_2.

C. Comparison to CVD on Silicon Wafers. ZN has been used as a thermal CVD precursor to ZrO_2 films grown in Si wafers.[15,57] In these experiments, ZrO_2 was deposited on 1 cm^2 Si(100) substrates that had been heated to remove adsorbed hydrogen. Depositions were studied in a high vacuum CVD system. Three regimes of growth were identified in the wafer CVD system: (i) a low temperature, reaction-limited regime (50−225 °C), in which the growth rate increases exponentially with increasing temperature; (ii) a moderate temperature, flux-limited regime (225−700 °C), in which the growth rate is independent of temperature; and (iii) a high-temperature regime (> 700 °C), in which the growth rate decreases with increasing temperature. The growth kinetics in this system were analyzed using a two-step kinetic model involving reversible ZN adsorption on the growth surface followed by irreversible precursor decomposition. An expression was developed to predict ZrO_2 deposition rates as functions of temperature and precursor partial pressure.

The wafer and particle CVD experiments were carried out under very different sets of conditions. Deposition onto aerosolized particles was studied at a single temperature, whereas deposition onto wafers was studied between 100 and 1000 °C. Also, the total reactor pressures were very different for the two systems: $\sim 1 \times 10^5$ Pa for the particle deposition system and 1×10^{-4} Pa in the high-vacuum reactor. Despite these differences, it is worthwhile to compare the two sets of measurements. For unheated particles, we observed a maximum growth rate of ~0.2 nm s^{-1}. For deposition onto a wafer at the same temperature (100 °C) and approximately the same precursor partial pressure, the linear deposition rate was quite comparable, ~0.5 nm s^{-1}. This good agreement may be fortuitous. Deposition onto a wafer is limited by the rate of precursor decomposition at 100 °C, whereas the pressure-dependent measurements suggest that the rate of ZrO_2 accumulation on a particle is limited by the gas−surface collision rate. Clearly, further work is necessary before a meaningful comparison of these two deposition systems is possible.

V. Conclusion

The experiments described in this study establish that chemical vapor deposition techniques can be adapted to grow inorganic layers on aerosolized silicon nanoparticles at atmospheric pressure. Using ZN as a precursor, coatings as thick as 0.9 nm were deposited onto the particles at 100 °C. These layers are believed to consist of ZrO_2, by analogy to what is known to occur in the wafer deposition systems. The ZrO_2 growth rates on particles are comparable to those on Si(100) wafers. Many of the observations reported in this work, for instance, of enhanced deposition upon particle preheating, require additional study. However, the general thrust of these experiments and their results clearly suggest, first, that thermal CVD onto aerosolized nanoparticles is a promising route to coated particles, and second, that TDMA is a useful probe of the kinetics of gas−nanoparticle reactions.

Acknowledgment. We thank Ying-Chih Liao and Joysura Basu for aid with the TEM imaging. This material is based on work supported by the National Science Foundation under Grant CHE-0094911. A.M.N. acknowledges partial support by the Integrative Graduate Education and Research Traineeship (IGERT) in Nanoparticle Science and Engineering at the University of Minnesota, which is funded by the National Science Foundation under Grant DGE-0114372, and by the University of Minnesota Dissertation Fellowship.

CM060883E

(55) Morita, Y.; Ishida, T.; Tokumoto, H. *Jpn. J. Appl. Phys.* **2002**, *41*, 2459−2462.
(56) Ha, J. S.; Park, K.-H.; Yun, W. S.; Ko, Y.-J.; Kim, S. K. *Surf. Sci.* **1999**, *426*, 373−383.
(57) Gladfelter, W. L.; Smith, R. C.; Burleson, D.; Taylor, C. J.; Roberts, J. T.; Campbell, S. A.; Hoilien, N.; Tiner, M.; Hegde, R.; Hobbs, C. *Mater. Res. Soc. Symp. Proc.* **2003**, *670*, K4 1/1−K4 1/10.